Geophysical Research Letters

RESEARCH LETTER
10.1029/2021GL092798

Using a Holistic Modeling Approach to Simulate Mud-Induced Periodic Stratification in Hyper-Turbid Estuaries

J. Schmidt[1] **and A. Malcherek**[1]

[1]Institute of Hydrosciences, Universität der Bundeswehr München, Munich, Germany

Key Points:

- A holistic sediment transport equation including sediment transport and consolidation is developed
- The rheological viscosity, the settling velocity, and a k-ω turbulence model are adapted to be valid in the region of the immobile mud
- A 1D vertical simulation of the holistic model is set up to simulate the flow and sediment processes in hyper-turbid estuaries

Correspondence to:
J. Schmidt,
johanna.schmidt@unibw.de

Citation:
Schmidt, J., & Malcherek, A. (2021). Using a holistic modeling approach to simulate mud-induced periodic stratification in hyper-turbid estuaries. *Geophysical Research Letters*, *48*, e2021GL092798. https://doi.org/10.1029/2021GL092798

Received 19 FEB 2021
Accepted 7 OCT 2021

Abstract This study focuses on a holistic modeling approach, in which water, fluid mud, and immobile mud are all calculated by only one set of equations. To integrate the immobile mud into this concept, a holistic transport equation including sediment transport and consolidation is developed. In some estuaries, extensive deepening and dredging resulted in tidal deformation and sediment import to such extent, that hyper-turbid conditions developed. Recent measurements from the Ems estuary show that the locations of interfaces between water, fluid mud, and consolidated mud vary during a tidal cycle. Conditions are varying from fully mixed to stably stratified. As a suitable case study for the holistic model, a 1D vertical numerical simulation of the Ems has been set up, which is able to qualitatively reproduce the observed vertical velocity, concentration, and velocity shear profile. The simulation shows mud-induced periodic stratification.

Plain Language Summary This study describes a 1D hydrodynamic-numerical model, which is called holistic as water, fluid mud, and immobile bed are solved by only one set of equations. Many estuaries are deepened and straightened to enable passage for ever-larger ships. In some estuaries, those artificial changes heavily influence the flow behavior and caused a shift to very high sediment concentrations resulting in thick layers of fluid mud. The presence of mud alters the flow- and turbulence behavior compared to pure water and subsequently must be included into the modeling equations. The model includes the immobile mud, where flow velocities and turbulence are zero. This is possible with a rearranged consolidation equation and the adaption of model parameters to be valid in cases of very high sediment concentration. Recent measurements from the Ems estuary show that the vertical concentration profile in the estuary strongly varies with time during one tidal cycle: There are phases of a stable fluid mud layer and phases of fully mixed conditions where no mud layer is present. As a possible application of the holistic model, a 1D vertical numerical simulation of the Ems estuary has been set up. The simulation results are in good agreement with field observations.

1. Introduction

In some estuaries, deepening and dredging caused a shift to very high sediment concentrations resulting in thick layers of fluid mud. Examples for such hyper-turbid estuaries are the Ems, Loire and Yangtze river. The Ems estuary is located at the German-Dutch border, see Figure 1a, with main riverine inputs from Ems (80 $m^3\ s^{-1}$) and Leda (24 $m^3\ s^{-1}$). Intensive dredging of the river has changed the flow profile such that the flood phase, compared to the ebb phase, is shorter, with higher velocities and acceleration. This led to an over 40 km long estuarine turbidity maximum (ETM) and the formation of a thick fluid mud layer with concentrations up to several tens to hundreds of grams per liter (Schrottke, 2006; Talke et al., 2009). Recent measurements of Becker et al. (2018a) show strongly varying concentration and velocity profiles over a tidal cycle. The processes occurring in the Ems are illustrated in Figure 1b which shows the concentration of suspended sediment over a tidal cycle in the estuary. During flood tide (position A), intense mixing occurs and the sediment concentration profile increases almost linearly from the free surface to the consolidated mud layer at the bottom. A shear layer is located near the bed, above the lower pronounced density gradient (lutocline). During slack water (position B) the sediment in the upper layer settles down and a two-layer flow forms, divided by a second lutocline. The rapid change in the concentration profile can be explained with turbulence damping due to stratification, which reduces vertical mixing and in turn leads to increased settling. The position of the largest density gradient moves upwards from the consolidated mud interface to the fluid mud-water interface. This restratification is related to damping of turbulent mixing processes.

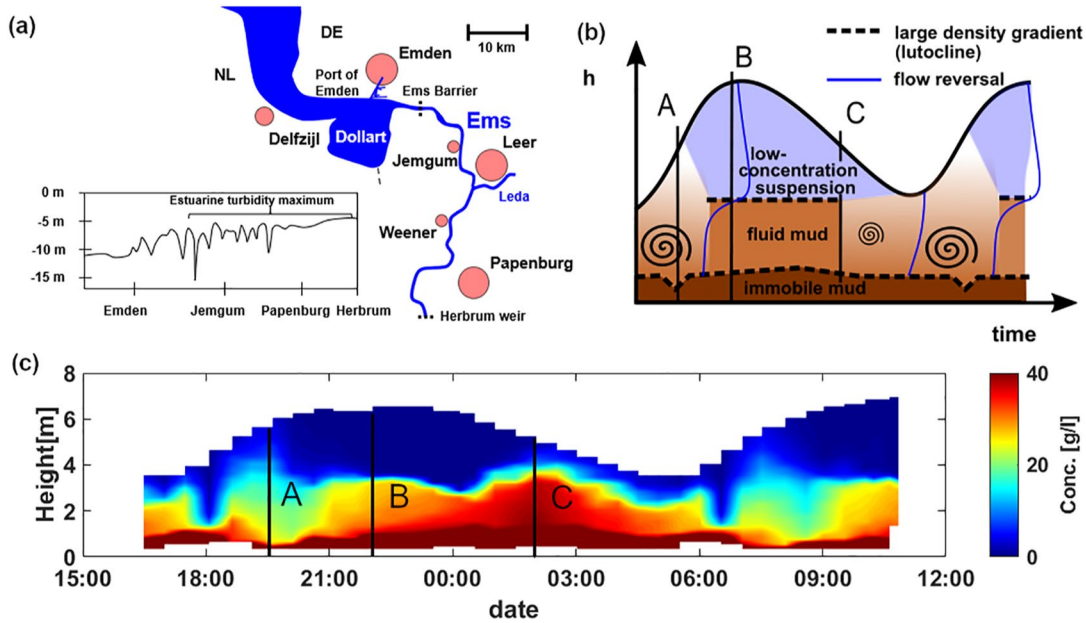

Figure 1. (a) Map of the Ems estuary and depth profile with location of the estuarine turbidity maximum (ETM). (b) Schematic picture of the vertical concentration profiles in the ETM. Position A shows a linear concentration profile due to strong mixing and a lutocline near the immobile bed. B shows stratified conditions with two lutoclines. During ebb tide, at position C, sediment concentrations remain high and less mixing compared to flood tide occurs. (c) Field observations of the vertical concentration profile from Becker et al. (2018a) with positions A, B, and C.

During ebb tide (position C) the flow velocities are usually not as large as during flood tide due to tidal asymmetry. Accordingly, the turbulent mixing is weaker compared to flood tide such that it cannot destroy the layered structure entirely.

Figure 1c shows the sediment concentration in the Ems estuary from optical backscatter measurements of Becker et al. (2018a). The sensor casts were collected every 30 min and the resulting vertical profiles are interpolated over time.

In order to investigate the impact of future measures to improve the situation in hyper-turbid estuaries, numerical models should be able to simulate the actual behavior of the system. When this is possible, the impact of planned measures can be studied using a numerical model before they are implemented.

Up to now, the interaction between fluid mud and tidal dynamics is seldom considered in hydrodynamic-numerical models for large-scale applications. The simulation of fluid mud dynamics is complex because of specific rheological properties of mud and a wide range of interactions between sediment characteristics and flow behavior. Le Normant et al. (1993) used the 3D free surface flow model TELEMAC-3D and included a sediment module to simulate cohesive sediment problems. The fluid mud dynamics were modeled by a depth-averaged approach, where fluid mud was represented by a constant, high viscosity. Le Normant (2000) applied this model for the Loire Estuary with a combination of a fluid mud module, erosion, deposition, and a vertical 1D bed consolidation module. Another fluid mud module is available in Delft3D, which calculates a separate mud layer with a constant sediment concentration (Winterwerp et al., 2002). However, those models neglect the rheological shear-thinning behavior of mud as a function of velocity shear and sediment concentration. Wehr and Malcherek (2012) simulated the complex non-Newtonian behavior of fluid mud with an isopycnal numerical model. This model concept can reproduce stably stratified flow conditions but not vertical mixing processes. Le Hir et al. (2001) introduced a continuous modeling approach, which combined water and mobile mud. Roland et al. (2012) developed a fluid mud module based on that continuous approach, which was coupled with the 3D flow models SHYFEM and SELFE. The model is able to reproduce stable stratification as well as vertical mixing of fluid mud. However, the immobile mud cannot be modeled and a detailed application and validation for an estuary are still needed. There is actually no 3D numerical model available which is able to simulate the described behavior of the sediment concentration

during a tidal cycle in the Ems. Therefore, as a first step, 1D vertical (1DV) models should be developed in order to understand the fundamental processes involved in that complex system.

In this study, a holistic approach is presented which uses the same set of fundamental balance equations for the water column as well as for the mud layer. The model can be regarded as an extension of the continuous model approach as it goes one step further by including the immobile mud. Deposition, erosion, and consolidation are inherent parts of the holistic equations.

2. Materials and Methods

The numerical model consists of four differential equations: The momentum balance, the sediment transport equation, and the two-equation k-ω turbulence model. The four equations are implemented using the finite volume method.

Assuming that the main processes take place in the vertical direction only, a 1DV numerical simulation has been set up. This means that horizontal divergence of transports is not considered. Furthermore, earth rotation, as well as internal pressure gradients due to horizontal density gradients are neglected. The suspended sediment is not treated as a separate phase but represented by a volumetric concentration and a settling velocity. The simulation does not include salinity, as salinity gradients in the Ems estuary are much smaller than those of sediment concentrations.

The 1D momentum equation in vertical (z) direction is

$$\frac{\partial u}{\partial t} = \frac{1}{\rho}\frac{\partial}{\partial z}\left[(\mu_{rh} + \mu_t)\frac{\partial u}{\partial z}\right] + gJ \tag{1}$$

with the fluid velocity in component along the estuary u, the rheological viscosity μ_{rh}, the turbulent viscosity μ_t, the gravitational acceleration g, and the resulting acceleration gJ, where J is the free surface gradient. The fluid density is calculated from $\rho = \phi_s\rho_s + (1-\phi_s)\rho_w$ with the volume fraction of solid particles $\phi_s = \frac{c}{\rho_s}$, the sediment concentration c, the sediment density $\rho_s = 2650\ \mathrm{kg\ m^{-3}}$ and the reference density of water $\rho_w = 1000\ \mathrm{kg\ m^{-3}}$. For the holistic model, the equations have to be valid in the water and in the immobile mud, which means for $0 \le \phi_s \le 1$. Combining rheological and turbulent viscosity was introduced by Le Hir et al. (2001). The rheological viscosity can be derived from measurements of fluid mud with a rheometer. The use of a rheological model based on specific measurements was implemented in a numerical simulation for the first time by Knoch and Malcherek (2011). The rheological viscosity is large when sediment concentrations are large and velocity shear is low. The turbulent viscosity is calculated by the turbulence model. In estuaries, a high turbulent viscosity results from strong turbulence due to vertical shear. By contrast, a high rheological viscosity suppresses turbulence and can lead to laminar flow conditions.

The adapted 1D sediment transport equation reads

$$\frac{\partial c}{\partial z} = \frac{\partial}{\partial z}\left[K_{hol}\frac{\partial c}{\partial z}\right] - \frac{\partial w_c c}{\partial z} \tag{2}$$

with the holistic diffusivity K_{hol}, which is later defined in Equation 13 and the settling velocity w_c. The classical solution of the sediment transport equation has the shape of a Rouse profile, see for example, Rouse (1937). The inclusion of several additional terms and processes, such as a rheological viscosity, hindered settling and turbulence damping, leads to a deviation from the typical Rouse profile. The following sections describe the properties of the model parameters within the holistic concept.

2.1. Rheological Viscosity

Newtonian fluids are defined by a linear dependence between the two parameters: shear rate (velocity shear) $\dot{\gamma}$ and shear stress τ. The observed flow curve in a rheometer is linear with the proportionality constant being the viscosity μ. Non-Newtonian fluids have a non-linear flow curve and/or can have a yield stress τ_y. The yield stress is the minimum shear stress that is necessary for flow to take place. Some fluids may have additional elastic and/or time-dependent characteristics. These are referred to as viscoelastic and thixotropic fluids, respectively.

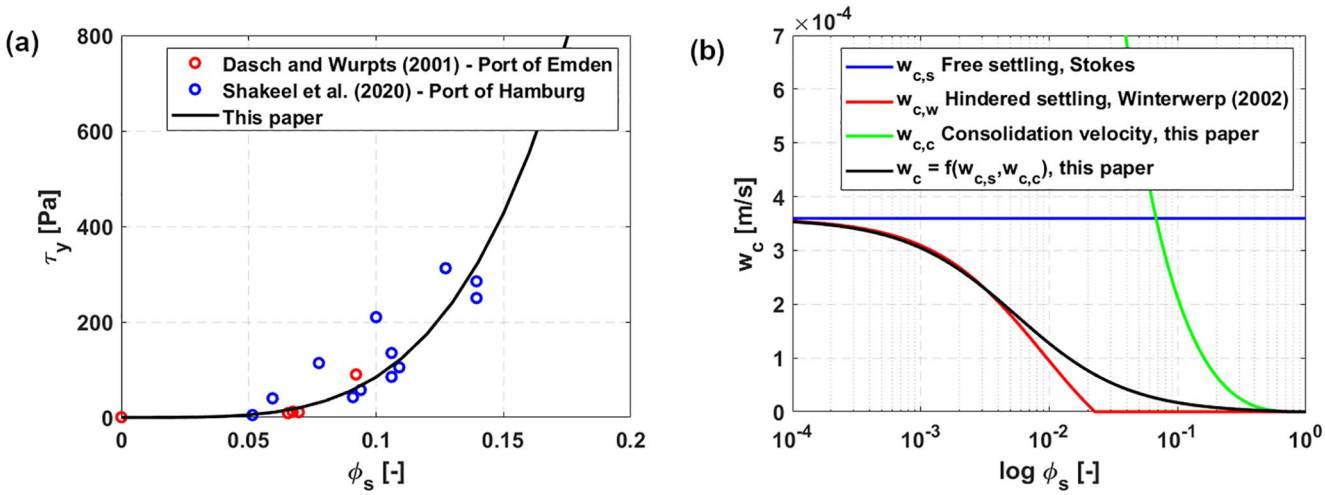

Figure 2. (a) Yield stress as a function of volume fraction of solid particles. This model uses $\tau_y = 8.44 \cdot 10^5$ Pa ϕ_s^4 as a possible parametrization for the Ems. Measurement data has been added from Dasch and Wurpts (2001) and Shakeel et al. (2020). (b) Settling velocities (absolute values) as a function of the volume fraction. The blue line is Stokes' settling velocity after Equation 10; the red line is hindered settling according to Equation 12, the green line is the consolidation settling velocity (Equation 8) that has been derived from the Gibson transport equation. The black line is the combined settling velocity (Equation 11). $d = d_{10} = 20 \cdot 10^{-6}$ m, $c_{gel} = 60$ g l^{-1}, $c_1 = 0.005$, $c_2 = 180$.

The yield stress increases with concentration, due to the increase in the number of interactions and the amplification of their intensity (Coussot & Piau, 1994). A simple approach to take this behavior into account is the Bingham model with an equation of the type $\tau = \tau_y(\phi_s) + \mu_y(\phi_s)\dot{\gamma}$ with the Bingham yield stress τ_y, the Bingham viscosity μ_y and the shear rate $\dot{\gamma}$ (O'Brien & Julien, 1988). The rheological viscosity is the shear stress τ divided by the shear rate $\dot{\gamma} = \max(|\frac{\partial u}{\partial z}|, 1 \cdot 10^{-6}\ \mathrm{s}^{-1})$. As the model is sensitive to the minimum shear rate, a value of $1 \cdot 10^{-6}$ s^{-1} or smaller is recommended.

A few decades ago, the dependence of yield stress on volume fraction for fine sediments was found to be $\tau_y = a_1 \phi_s^{\ r}$ with $4 < r < 5$ (Migniot, 1968). Most authors, such as O'Brien and Julien (1988), Coussot and Piau (1994), Fonseca et al. (2019), and Carneiro et al. (2020), use an exponential function of the type $\tau_y = a_2 \exp(b_2 \phi_s)$ instead of a power relation. This type does not result in $\tau_y = 0$ for $\phi_s = 0$ but in $\tau_y = a_2$. Considering a holistic model, this means that water ($\phi_s = 0$) has a non-zero Bingham yield stress, which is not correct. For this reason, we adopt the power relation where in the case of $\phi_s = 0$, there is no yield stress. There exist many yield stress measurements of mud samples for different densities and locations. Figure 2a compares the yield stress from different estuaries as a function of the volume fraction of solid particles. A least squares fit was applied to the data shown. We set $r = 4$ and achieved $a_1 = 8.44 \cdot 10^5$ Pa ($R^2 = 0.76$).

The dependence of the Bingham viscosity on the solid content is $\mu_y = \mu_m \exp(b_1 \phi_s)$ with $b_1 \approx 20$ (Malcherek & Cha, 2011). This relation indicates that in the case of no sediment, where $\phi_s = 0$, the rheological viscosity yields the molecular viscosity $\mu_m = 1 \cdot 10^{-3}$ Pa s of water. The rheological viscosity can be calculated with the equation

$$\mu_{rh} = \frac{a_1 \phi_s^{\ r}}{\dot{\gamma}} + \mu_m \exp(b_1 \phi_s). \tag{3}$$

The rheological viscosity increases with higher volume fractions and decreases with increasing shear rate. The latter occurs due to the shear-thinning behavior of fluid mud. The rheological viscosity as defined by Equation 3 is a possible parametrization for mud in the Ems estuary and is valid for $0 \le \phi_s \le 1$.

2.2. Turbulence Model

Turbulence models are used to calculate the turbulent viscosity in a fluid that affects several properties, for example, the velocity in the flow. Generally, in a stationary shear flow without sediment, a logarithmic velocity profile develops. Very close to the wall, in the viscous sublayer, the velocity profile is however linear.

The universal velocity profile represents the turbulent flow (log-law region) as well as the laminar flow (viscous sublayer). The presence of fluid mud enlarges the viscous sublayer, that is, the region where the flow is laminar (Li & Gust, 2000). Having said that, the chosen turbulence model should be able to calculate the log-law region as well as the viscous sublayer. If the immobile mud is considered, the turbulence has to be zero as there is no movement and therefore no possible production of turbulent kinetic energy.

The k-ω turbulence model as developed by Wilcox (1988) consists of two differential equations, one for the turbulent kinetic energy k and one for the dissipation rate ω. In contrast to the k-ϵ turbulence model (e.g., Launder & Spalding, 1974), the k-ω model is able to calculate the viscous sublayer without introducing additional damping functions (Wilcox, 2010). Furthermore, it has the ability to consider the Stokes' wall condition ($u_b = 0$, $k_b = 0$) in the bottom boundary condition for ω (Wilcox, 2010). Within this modeling concept, as ω has a finite value at closed boundaries where the turbulent kinetic energy is zero, it cannot be interpreted as a dissipation rate itself and is for this reason defined as the potential of a dissipation rate. Chmiel et al. (2020) have shown how the k-ω model is able to work in fluid mud and sediment layers and results in $k = 0$ for high concentrations. The turbulence model by Wilcox (1988) and adapted from Chmiel et al. (2020) is

$$\frac{\partial k}{\partial t} = \frac{1}{\rho}\frac{\partial}{\partial z}\left[(\mu_{rh} + \mu_t \sigma^\star)\frac{\partial k}{\partial z}\right] + P_k - \epsilon + G\,, \tag{4}$$

$$\frac{\partial \omega}{\partial t} = \frac{1}{\rho}\frac{\partial}{\partial z}\left[(\mu_{rh} + \mu_t \sigma)\frac{\partial \omega}{\partial z}\right] + \alpha\frac{\omega}{k}P_k - \beta\omega^2\,. \tag{5}$$

The coefficients of the turbulence model are $\sigma^\star = \sigma = \frac{1}{2}$, $\alpha = \frac{5}{9}$, $\beta = \frac{3}{40}$ and $\beta^\star = \frac{9}{100}$. The turbulent viscosity μ_t results from

$$\mu_t = \frac{\nu_t}{\rho} = \frac{1}{\rho}\frac{k}{\omega}.$$

The rheological viscosity is considered not only in the momentum balance but also in the turbulence model. The production of k, P_k, is obtained from

$$P_k = \nu_t\left(\frac{\partial u}{\partial z}\right)^2,$$

the dissipation is

$$\epsilon = \beta^\star k\omega\,,$$

and the buoyancy term G is calculated from

$$G = \frac{\nu_t}{\sigma_s}\frac{g}{\rho}\frac{\partial \rho}{\partial z}\,,$$

where σ_s is the turbulent Schmidt number. P_k is high in regions of high shear rates $\frac{\partial u}{\partial z}$. This is usually the case above the lutocline, where changes in velocity are large. G is negative in the case of stably stratified flows as $\frac{\partial \rho}{\partial z}$ is negative. This leads to a reduction of k, which means the destruction of turbulence.

2.3. A Holistic Sediment Transport Equation

Sediment transport and consolidation affect each other. If sediment particles settle due to a decrease in turbulence, the sediments form a highly concentrated suspension near the bottom. If shear forces remain low, the suspension starts to consolidate. If shear forces are high, sediment that is already consolidated can be liquefied and entrained into the water column. Consequently, to account for the dependence of both processes, they will be modeled together in one single differential equation. To do so, the Gibson consolidation equation needs to be rearranged such that it has the same mathematical shape as the classical sediment transport equation. This means that it consists of an advective and a diffusive term for the sediment concentration c. The one-dimensional consolidation equation from Gibson et al. (1967) is

$$\frac{\partial \phi_s}{\partial t} + \frac{\partial}{\partial z}\left[k_f(1-\phi_s)\left(1-\frac{\rho_s}{\rho_w}\right)\phi_s^2\right] = \frac{\partial}{\partial z}\left[\frac{k_f(1-\phi_s)\phi_s}{\rho_w g}\frac{\partial \sigma'}{\partial z}\right], \tag{6}$$

where k_f is the permeability and σ' the effective stress. Merckelbach (2000) obtained $\sigma' = A_\sigma \phi_s^{B_\sigma} - C_\sigma$ from measurements for the effective stresses of soft mud layers. Derivation by z leads to $\frac{\partial \sigma'}{\partial z} = A_\sigma \phi_s^{B_\sigma - 1} \frac{\partial \phi_s}{\partial z}$, which can be included in Equation 6. The parameters are $(3.9 \cdot 10^8 \leq A_\sigma \leq 4.1 \cdot 10^9)$ Pa and $7.1 \leq B_\sigma \leq 8.0$. Furthermore, substituting $\phi_s = \frac{c}{\rho_s}$ yields

$$\frac{\partial c}{\partial t} + \frac{\partial}{\partial z}\left[\underbrace{k_f (1-\phi_s)\phi_s \left(1 - \frac{\rho_s}{\rho_w}\right)}_{w_{c,c}} c\right] = \frac{\partial}{\partial z}\left[\underbrace{\frac{k_f (1-\phi_s)}{\rho_w g} A_\sigma \phi_s^{B_\sigma}}_{K_c} \frac{\partial c}{\partial z}\right]. \tag{7}$$

This new equation now has the shape of the classical sediment transport equation and, as a result, leads to a formulation for a consolidation settling velocity and a consolidation diffusivity. The consolidation settling velocity is

$$w_{c,c} = k_f (1-\phi_s)\phi_s \left(1 - \frac{\rho_s}{\rho_w}\right). \tag{8}$$

The consolidation diffusivity is

$$K_c = \frac{k_f (1-\phi_s)}{\rho_w g} A_\sigma \phi_s^{B_\sigma}. \tag{9}$$

The permeability k_f is derived from Kozeny (1927) and Carman (1937) as

$$k_f = c_1 \frac{g d_{10}^2}{\nu_m} \frac{(1-\phi_s)^3}{\phi_s^2}$$

with $0.003 < c_1 < 0.0055$, the molecular kinematic viscosity $\nu_m = 1 \cdot 10^{-6}$ m^2 s^{-1} and the diameter d_{10} being the 10% quantile of particle diameter.

2.4. From Settling to Consolidation

The next step is to establish a relation between settling in the water column and settling due to consolidation. Fluid mud can be described as fine-grained sediment particles in a water suspension. As sediment has a higher density than water, the particles settle within the water column. For a single, spherical particle with the diameter d, Stokes' formula for the settling velocity

$$w_{c,s} = \frac{1}{18} \frac{g d^2}{\nu_m} \left(1 - \frac{\rho_s}{\rho_w}\right) \tag{10}$$

is valid. However, falling particles generate a return flow and influence other particles in the vicinity. Thus, the settling velocity of the suspension decreases by a factor $(1-\phi_s)$. When comparing Equations 8 and 10 similarities become obvious. In order to achieve a transition for both settling velocities, a blending is suggested such that

$$w_c = (1-\phi_s)\left(1 - \frac{\rho_s}{\rho_w}\right) \frac{g}{\nu_m} \min\left(c_1 \frac{d_{10}^2 (1-\phi_s)^3}{\phi_s}, \frac{d^2}{18} \frac{1}{(1+c_2\phi_s)}\right). \tag{11}$$

The first part of Equation 11 is always negative and consists of those parts that are identical in both $w_{c,s}$ (with return flow effects included) and $w_{c,c}$. The second part is a minimum function of the remaining parts with an additional term $\frac{1}{(1+c_2\phi_s)}$ for the Stokes' settling velocity. The term represents hindered settling, which is typical for high concentration suspensions. Winterwerp (2002) states three reasons for hindered settling. First, the return flow of a particle, which reduces the settling velocity of surrounding particles. Second, the increase of the viscosity of the suspension and, third, enhanced buoyancy due to increased concentration. All effects reduce the settling velocity with increasing sediment concentration, which leads to

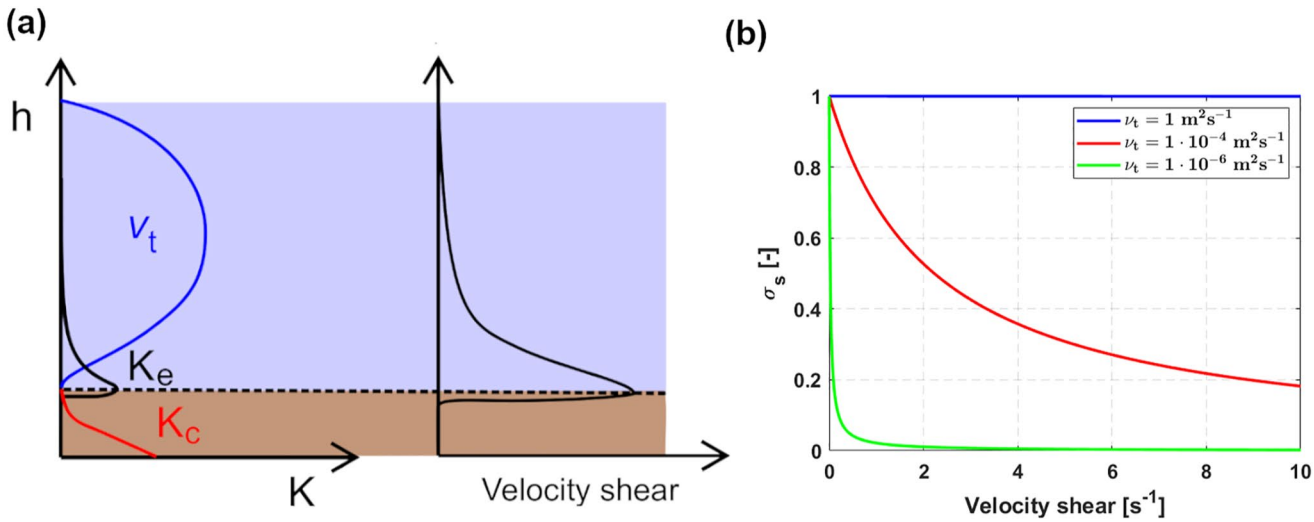

Figure 3. (a) Scheme of diffusivity and velocity shear in the water column and immobile mud. In contrast to the velocity, the velocity shear is non-zero at the pronounced density gradient (dashed line). (b) Turbulent Schmidt number from Equation 14, where $l_c = 6.7 \cdot 10^{-3}$ m.

$$w_{c,w} = w_{c,s} \frac{\left(1 - \min\left(1, \frac{c}{c_{gel}}\right)\right)(1 - \phi_s)}{1 + 2.5\frac{c}{c_{gel}}}. \tag{12}$$

The gelling concentration c_{gel} is referred to as the concentration at which the flocs exist as a room-filling network (Camenen & van Pham Bang, 2011; Winterwerp & van Kesteren, 2004). It can be regarded as the transition from the hindered settling regime to consolidating mud (Dankers & Winterwerp, 2007). The settling velocity obtained from Equation 12 becomes zero if $c = c_{gel}$. Considering consolidation, the settling velocity should not be zero at that point, but equal to the velocity of the consolidating mud.

The settling velocities from Stokes, Winterwerp, the consolidation velocity, and the applied transition are shown in Figure 2b. The combined formula for w_c shows the requested behavior for mud. At higher volume fractions or concentrations, respectively, the settling velocity decreases and merges into $w_{c,c}$. Finally, if the volume fraction $\phi_s = 1$, the settling velocity becomes zero. The achieved function (Equation 11) has a similar shape as the approach from Equation 12, but we use Equation 11 in the holistic model because the formula includes the consolidation velocity and consists of neither a gelling concentration nor a discontinuity in the slope.

2.5. A Holistic Diffusivity Approach

The classical sediment transport equation consists only of the turbulent diffusivity K_t. For the holistic approach a consolidation diffusivity K_c, see Equation 9, exists in the immobile mud where the turbulent viscosity is zero. Morphodynamics and fluid mechanics are usually modeled separately and connected via the sediment flux in between. Sediment is eroded when the shear stress is higher than the erosion shear strength. In this holistic approach, erosion can only be included as a diffusivity as there is no separate equation. Accordingly, an erosion diffusivity $K_e = l_c^2\dot{\gamma}$ is added. It is proportional to the absolute value of the velocity shear and a proportionality constant which has been denoted as erosion mixing length l_c. Figure 3a illustrates a water and immobile mud layer with ν_t, K_e and K_c. In contrast to the flow velocity, the velocity shear is non-zero at the interface between water and bed. For that reason, K_e must be proportional to the velocity shear.

We define the holistic diffusivity as

$$K_{hol} = K_c + K_t, \tag{13}$$

with $K_t = \nu_t + K_e$. The ratio between turbulent viscosity and diffusivity $\sigma_s = \frac{\nu_t}{K_t}$ is the turbulent Schmidt number σ_s. According to the relations defined above

$$\sigma_s = \frac{\nu_t}{\nu_t + K_e}. \tag{14}$$

As illustrated in Figure 3b, σ_s decreases with increasing velocity shear and decreasing turbulent viscosity. Typically, σ_s is a function that is derived from second-order turbulence models, depending on shear and stratification. Here, the turbulent Schmidt number is also a function but not derived from second-order closure but from adding the erosion diffusivity to the turbulent viscosity. Consequently, the relation between mixing of momentum and mixing of masses is modified. Further research is needed to verify this assumption. This modification also influences the buoyancy term, which is typically not only present in Equation 4 but also in Equation 5. When the buoyancy term is added, another parameter that is dependent on the Schmidt number function arises. Again, as the relation between mixing of momentum and mixing of sediment was modified, this is also subject to further research.

3. Simulation of the Ems Model

The aim of the simulation is to reproduce the processes occurring in the Ems estuary, especially to simulate mud-induced periodic stratification and to show that the model includes the immobile bed. The 1DV model solves the differential equations for velocity, sediment concentration, and the turbulent quantities k and ω. The model Equations 1, 2, 4, and 5 are discretized using the finite volume method. The water level h and the gravitational acceleration gJ (where $J = \frac{dh}{dx}$) are predefined. In order to account for the time-dependent water level, tidal constituents M2 and M4 are considered, as they are the most dominant at the study site. The M4 component has a phase shift that yields the characteristic asymmetrical profile of the Ems. The flood phase is shorter and exhibits higher velocities compared to the ebb phases. The vertical resolution is $\Delta z = 0.237$ m; the grid is equidistant except for the last cell, which is adapted to the current water level. We use Equation 3 for the rheological viscosity, Equation 11 for the settling velocity, and Equation 13 for the holistic diffusivity. An erosion mixing length of $l_c = 6.7 \cdot 10^{-3}$ m yields the best model fit to the observations from the Ems estuary (Table 1).

The 1DV model calculates the velocity, the sediment concentration, and the turbulent parameters over the vertical simulation domain. The total simulation time is 5 days, the time step Δt is 10 s. The simulation reaches a steady state after an initial time period of three tidal cycles. The initial concentration in each cell is $c_0 = 28\ \mathrm{g\ l^{-1}}$. The boundary conditions at the bottom are $u_b = 0$, $k_b = 0$ and $\omega_b = 2500\frac{\nu_m}{k_s^2}$ with the bottom roughness $k_s = 3.2 \cdot 10^{-3}$ m. No-flux boundary conditions are applied for concentration at the bottom and the free surface. At the free surface no-flux boundary conditions for u and k are chosen, which means that there is no wind stress acting on the surface. This is justified as the concurrent field observations were obtained on days of little wind. However, wind forces can be added to the model in future simulations if needed. The value for ω at the free surface is $\omega_s = 0.1\ \mathrm{s^{-1}}$. This value is chosen to be small, to reduce the flow velocity at the free surface. The model has been implemented in MATLAB. The simulation results are most sensitive to the vertical resolution, the settling velocity, the rheological viscosity, the erosion mixing length, and the initial sediment concentration.

4. Results and Discussion

Figure 4a shows the simulation results of the vertical concentration profile over a time period of 19 hr in analogy to Figure 1c. Figure 4b compares the concentration, velocity, and velocity shear profiles for the positions A, B, and C for measurements and simulation. The water level periodically rises and falls similarly to the actual water level. At position A the sediment is distributed over the entire water column and the immobile mud layer is the thinnest among all three positions because of enhanced erosion during flood tide. The velocities at position A are high and directed upstream, and the highest shear is located close to the immobile mud. The simulation deviates from the linear concentration profile from the measurements. A possible explanation is that in the simulation only M2 and M4 tidal components are considered. As a consequence, the beginning of flood tide sets in less abruptly and leads to less acceleration and less mixing

Table 1
List of Important Mathematical Symbols and Parameters for the Ems Model

Symbol	Definition	Value (Ems model)	Unit
c	Sediment concentration		$kg\ m^{-3}$
c_{gel}	Gelling concentration		$kg\ m^{-3}$
d	Particle diameter	$20 \cdot 10^{-6}$	m
d_{10}	Particle diameter at 10% sieve passage	$20 \cdot 10^{-6}$	m
g	Gravitational acceleration		$m\ s^{-2}$
G	Buoyancy term		$m^2\ s^{-3}$
J	Free surface gradient		–
k	Turbulent kinetic energy		$m^2\ s^{-2}$
k_f	Permeability		$m\ s^{-1}$
k_s	Bottom roughness	$3.2 \cdot 10^{-3}$	m
K_c	Consolidation diffusivity	Equation 9, $A_\sigma = 4 \cdot 10^8$ Pa, $B_\sigma = 7.5$	$m^2\ s^{-1}$
K_e	Erosion diffusivity		$m^2\ s^{-1}$
K_{hol}	Holistic diffusivity		$m^2\ s^{-1}$
K_t	Turbulent diffusivity		$m^2\ s^{-1}$
l_c	Erosion mixing length	$6.7 \cdot 10^{-3}$	m
P_k	Production of turbulent kinetic energy		$m^2\ s^{-3}$
u	Velocity in x-direction		$m\ s^{-1}$
w_c	Settling velocity	Equation 11, $c_1 = 0.005$, $c_2 = 180$	$m\ s^{-1}$
z	Vertical coordinate		m
Δt	Time step	10	
Δz	Mesh spacing	0.237	m
$\dot{\gamma}$	Shear rate		s^{-1}
μ_m	Molecular viscosity	$1 \cdot 10^{-3}$	$Pa\ s$
μ_{rh}	Rheological viscosity	$\frac{\tau_y}{\dot{\gamma}} + \mu_y$	$Pa\ s$
μ_t	Turbulent viscosity		$Pa\ s$
μ_y	Bingham viscosity	$\mu_m \exp(20\ \phi_s)$	$Pa\ s$
ν_m	Molecular kinematic viscosity	$1 \cdot 10^{-6}$	$m^2\ s^{-1}$
ν_{rh}	Rheological kinematic viscosity		$m^2\ s^{-1}$
ν_t	Turbulent kinematic viscosity		$m^2\ s^{-1}$
ρ	Bulk density		$kg\ m^{-3}$
ρ_s	Sediment density	2,650	$kg\ m^{-3}$
ρ_w	Density of water	1,000	$kg\ m^{-3}$
σ_s	Turbulent Schmidt number		–
τ	Shear stress		Pa
τ_y	Bingham yield stress	$8.44 \cdot 10^5\ \phi_s^4$	Pa
ϕ_s	Volume fraction of particles	$\frac{c}{\rho_s}$	–
ω	Potential of a dissipation rate		s^{-1}

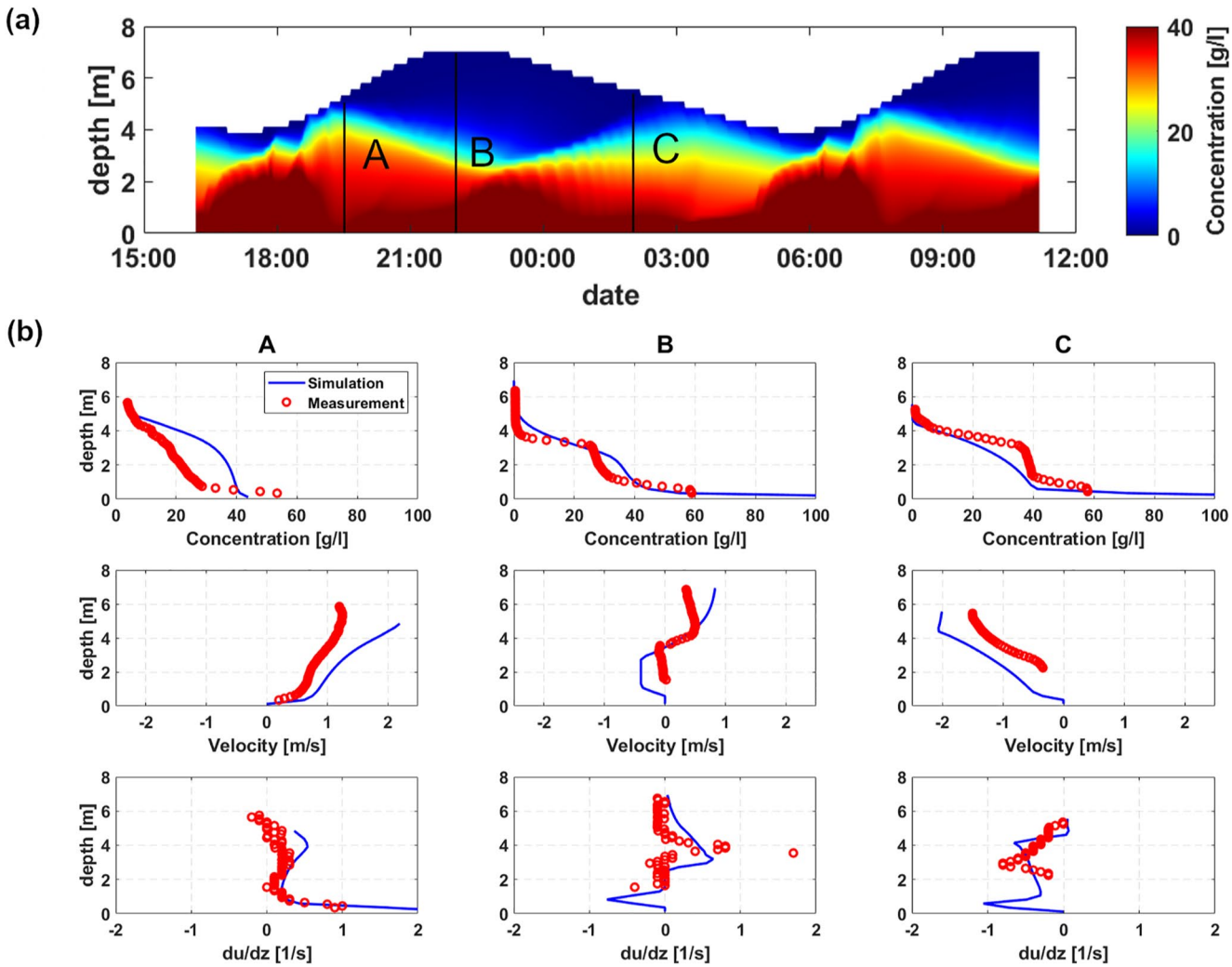

Figure 4. (a) Simulation results of the vertical concentration profile from the 1DV model. The simulation results cover the same time range as the field observations shown in Figure 1c. (b) Comparison of velocity, concentration and velocity shear profiles at positions A, B, and C for measurement and simulation data.

compared to the field observations. At position B, the simulation qualitatively shows the step in the concentration profile, which indicates the development of a lutocline. The concentration values in the fluid mud layer ($c = 35$ g l^{-1}) are slightly higher than the actual values. The velocity profile at the same position consists of lower velocities in the fluid mud layer and higher velocities above the lutocline. The velocities in the fluid mud are overestimated by the simulation, which could be due to too low rheological viscosities. The velocity shear yields similarly high values above the upper and the lower lutocline. The field observations show higher velocity shear above the upper lutocline but the general behavior is well captured. Accordingly, the simulation is able to reproduce the stratification of fluid mud. During ebb tide (position C), the velocities are directed downstream and the position of highest shear is right above the lower lutocline. The measurements deviate from that, as the upper lutocline still exists at position C. The measurement data does not provide insight into velocity shear data close to the bottom, which is probably lower than the calculated values. The too rapid destruction of the lutocline with the onset of ebb tide is probably due to several effects. First, the ebb tide starts too early compared to the measured data, causing the flow velocities to be too high. Second, the neglect of flocculation processes could also play a role: Macroflocs, which have higher settling velocities, could form during slack water and stabilize the lutocline at the beginning of the ebb phase. The simulation results should also be considered from the point of view of the 1D model: A vertical 1D model

is only capable to simulate vertical transport processes (settling, entrainment, deposition, and erosion). It is not valid when horizontal transport processes are dominant in an estuarine system.

Although there are more advanced rheological models, turbulence models, or settling velocity approaches than those presented here, the simulation is able to qualitatively reproduce the mud dynamics in the Ems estuary. These parameters, which are usually determined by field or laboratory measurements, are subject to large uncertainties. The 1D model can therefore be considered as a useful tool to validate these parameters, which can then be implemented in 2D and 3D simulations. The total number of parameters used in our simulation was kept to a minimum, and the simulation of the Ems presented here does not require a separate fluid mud or sediment module. Overall, the simulation shows mud-induced periodic stratification and the results are in fair agreement with the actual data.

5. Summary and Conclusions

A model approach has been presented which consists of four differential equations to calculate the flow velocity, concentration, and turbulence profile in a hyper-turbid estuary. The Gibson equation for consolidation was rearranged to the same structure as the sediment transport equation. This procedure allows to include the simulation of sediment transport processes from settling to consolidation in one single equation. The model is valid in the water column, the moving mud as well as in the immobile bed. In that way, the model can be regarded as holistic. In classical models, the described layers are separated, and connected with empirical parametrizations.

A simulation of the hyper-turbid Ems estuary is presented and the simulation results show that the model can reproduce mud-induced periodic stratification. The simulation results are comparable to recent measurements in the Ems estuary for the concentration profile, flow velocity, and velocity shear. The latter is an indicator for the production of turbulence and, on that account, turbulence itself. All quantities are also calculated in the immobile bed, where the flow velocity and turbulence are zero and concentrations are very high.

The holistic modeling approach is applicable to various problems, for example to studies of sediment settling. To simulate a settling column for fine sediments, the free surface gradient in the momentum balance has to be set to zero. A homogeneous concentration can be defined at the initial time step. With time, the sediment settles and consolidates. This means that the model setup can be used to calibrate model parameters for sediment settling and consolidation.

Data Availability Statement

V1.1 of the model code of the 1DV model used for the simulation is preserved at Malcherek and Schmidt (2021). The measurement data used for comparison is available through Becker et al. (2018b).

Acknowledgment
This work was partially funded by the German Federal Waterways Engineering and Research Institute (BAW). Open access funding enabled and organized by Projekt DEAL.

References

Becker, M., Maushake, C., & Winter, C. (2018a). Observations of mud-induced periodic stratification in a hyperturbid estuary. *Geophysical Research Letters*, *45*(11), 5461–5469. https://doi.org/10.1029/2018GL077966

Becker, M., Maushake, C., & Winter, C. (2018b). Vertical profiles of current velocity, suspended sediment concentration, and salinity during one tidal cycle at Jemgum, Ems estuary, Germany, supplement to: Becker, Marius; Maushake, Christian; Winter, Christian (2018): Observations of mud-induced periodic stratification in a hyperturbid estuary. *Geophysical Research Letters*, *45*(11), 5461–5469. PANGAEA - Data Publisher for Earth & Environmental Science. https://doi.org/10.1594/PANGAEA.890517

Camenen, B., & van Pham Bang, D. (2011). Modelling the settling of suspended sediments for concentrations close to the gelling concentration. *Continental Shelf Research*, *31*(10), S106–S116. https://doi.org/10.1016/j.csr.2010.07.003

Carman, P. C. (1937). Fluid flow through granular beds. *Transactions of the Institution of Chemical Engineers*, *15*, 150–166.

Carneiro, J. C., Gallo, M. N., & Vinzón, S. B. (2020). Detection of fluid mud layers using tuning fork, dual-frequency echo sounder, and chirp sub-bottom measurements. *Ocean Dynamics*, *70*(4), 573–590. https://doi.org/10.1007/s10236-020-01346-8

Chmiel, O., Naulin, M., & Malcherek, A. (2020). Combining turbulence and mud rheology in a conceptual 1DV model – An advanced continuous modeling concept for fluid mud dynamics. *Die Küste*, *89*. https://doi.org/10.18171/1.089101

Coussot, P., & Piau, J. M. (1994). On the behavior of fine mud suspensions. *Rheologica Acta*, *33*(3), 175–184. https://doi.org/10.1007/BF00437302

Dankers, P., & Winterwerp, J. C. (2007). Hindered settling of mud flocs: Theory and validation. *Continental Shelf Research*, *27*(14), 1893–1907. https://doi.org/10.1016/j.csr.2007.03.005

Dasch, W., & Wurpts, R. (2001). Isovics as useful parameters for describing sedimentation. *Terra et Aqua*, *82*, 3–7.

Fonseca, D. L., Marroig, P. C., Carneiro, J. C., Gallo, M. N., & Vinzón, S. B. (2019). Assessing rheological properties of fluid mud samples through tuning fork data. *Ocean Dynamics*, *69*(1), 51–57. https://doi.org/10.1007/s10236-018-1226-9

Gibson, R. E., England, G. L., & Hussey, M. J. L. (1967). The theory of one-dimensional consolidation of saturated clays. *Géotechnique*, *17*, 261–273. https://doi.org/10.1680/geot.1967.17.3.261

Knoch, D., & Malcherek, A. (2011). A numerical model for simulation of fluid mud with different rheological behaviors. *Ocean Dynamics*, *61*(2–3), 245–256. https://doi.org/10.1007/s10236-010-0327-x

Kozeny, J. (1927). Über kapillare Leitung des Wassers im Boden. *Sitzungsber Akademie der Wissenschaften in Wien*, *136*(2a), 271–306.

Launder, B. E., & Spalding, D. B. (1974). The numerical computation of turbulent flows. *Computer Methods in Applied Mechanics and Engineering*, *3*(2), 269–289. https://doi.org/10.1016/0045-7825(74)90029-2

Le Hir, P., Bassoullet, P., & Jestin, H. (2001). Application of the continuous modeling concept to simulate high-concentration suspended sediment in a macrotidal estuary. *Proceedings in Marine Science*, *3*, 229–247. https://doi.org/10.1016/S1568-2692(00)80124-2

Le Normant, C. (2000). Three-dimensional modelling of cohesive sediment transport in the Loire estuary. *Hydrological Processes*, *14*(13), 2231–2243. https://doi.org/10.1002/1099-1085(200009)14:13<2231::aid-hyp25>3.0.co;2-#

Le Normant, C., Lepeintre, F., Teisson, C., Malcherek, A., Markofsky, M., & Zielke, W. (1993). *Three dimensional modelling of estuarine processes*. Project Report (1). MAST Days and Euromar Market.

Li, M. Z., & Gust, G. (2000). Boundary layer dynamics and drag reduction in flows of high cohesive sediment suspensions. *Sedimentology*, *47*(1), 71–86. https://doi.org/10.1046/j.1365-3091.2000.00277.x

Malcherek, A., & Cha, H. (2011). *Zur Rheologie von Flüssigschlicken: Experimentelle Untersuchungen und theoretische Ansätze*. Shaker-Verlag.

Malcherek, A., & Schmidt, J. (2021). *1DV-Holistic-Ems-Model: A holistic model to simulate mud-induced periodic stratification in hyper-turbid estuaries*. Zenodo. https://doi.org/10.5281/ZENODO.5533535

Merckelbach, L. M. (2000). *Consolidation and strength evolution of soft mud layers* (Dissertation). Delft University of Technology.

Migniot, C. (1968). Étude des propriétés physiques de différentes sédiments très fins et de leur comportement sous des actions hydrodynamiques. *La Houille Blanche*, *7*, 591–620. https://doi.org/10.1051/lhb/1968041

O'Brien, J. S., & Julien, P. Y. (1988). Laboratory analysis of mudflow properties. *Journal of Hydraulic Engineering*, *114*(8), 877–887. https://doi.org/10.1061/(ASCE)0733-9429

Roland, A., Ferrarin, C., Bellafiore, D., Zhang, Y. J., Sikric, M. D., Zanke, U., & Umgiesser, G. (2012). *Über Strömungsmodelle auf unstrukturierten Gitternetzen zur Simulation der Dynamik von Flüssigschlick*. Retrieved from https://henry.baw.de/bitstream/20.500.11970/101668/1/k079102.pdf

Rouse, H. (1937). Modern conceptions of the mechanics of fluid turbulence. *Transactions of the American Society of Civil Engineers*, *102*(1), 463–505. https://doi.org/10.1061/TACEAT.0004872

Schrottke, K. (2006). *Dynamik fluider Schlicke im Weser und Ems-Ästuar - Untersuchung und Analysen zum Prozessverständnis*. BAW/BfG Kolloqium.

Shakeel, A., Kirichek, A., & Chassagne, C. (2020). Rheological analysis of mud from Port of Hamburg, Germany. *Journal of Soils and Sediments*, *20*, 2553–2562. https://doi.org/10.1007/S11368-019-02448-7

Talke, S. A., de Swart, H. E., & Schuttelaars, H. M. (2009). Feedback between residual circulations and sediment distribution in highly turbid estuaries: An analytical model. *Continental Shelf Research*, *29*(1), 119–135. https://doi.org/10.1016/j.csr.2007.09.002

Wehr, D., & Malcherek, A. (2012). Numerical simulation of fluid mud dynamics - The isopycnical model MudSim. *Die Küste*, *79*, 1–52.

Wilcox, D. C. (1988). Reassessment of the scale-determining equation for advanced turbulence models. *AIAA Journal*, *26*(11), 1299–1310. https://doi.org/10.2514/3.10041

Wilcox, D. C. (2010). *Turbulence modeling for CFD*. DCW Industries.

Winterwerp, J. C. (2002). On the flocculation and settling velocity of estuarine mud. *Continental Shelf Research*, *22*(9), 1339–1360. https://doi.org/10.1016/s0278-4343(02)00010-9

Winterwerp, J. C., & van Kesteren, W. (2004). *Introduction to the physics of cohesive sediment in the marine environment*. Elsevier Science Publishing Co.

Winterwerp, J. C., Wang, Z. B., van Kester, J. A. T. M., & Verweij, J. F. (2002). Far-field impact of water injection dredging in the Crouch River. *Maritime Engineering*, *154*(4), 285–296. https://doi.org/10.1680/maen.154.4.285.38905